Numerical Modeling and Simulation of Rooftop Thermal Photovoltaic Chimney For Buildings' Electrical Energy Generation And Passive Cooling.

Yawovi Nougbléga[1,2,*], Georges Kibalo Tchamie[1], Seydou Ouedraogo[3]

[1] Laboratoire Sur l'Energie Solaire /Groupe Phénomènes de Transfert et Energétique, Université de Lomé, 01 Lomé, BP 1515
[2] Regional Centre of Excellence on Electricity Management (CERME), University of Lomé
[3] Département de Génie Electrique, Institut Universitaire de Technologie, Université Nazi BONI, Burkina-Faso
*Correspondence:e-mail: nycogl@yahoo.fr; Tel.: +22890218796

Abstracts: The present study consisted mainly of making the thermal and dynamic analysis of the fluid flows in mixed convection in the chimney integrated into the building with an upper-covered horizontal hybrid thermal photovoltaic collector on a slab roof. The governing equations discretized by the finite difference method resulted in the systems of tri-diagonal algebraic equations, which were solved by Thomas' algorithm and Gauss Seidel's iterative method. Numerical solutions are presented for various geometrical aspect ratios, Rayleigh, and Reynolds numbers. The results are presented in terms of streamlines, isotherms, velocity, heat transfer intensity, and PV cells' electrical efficiency versus the governing control parameters in detail.

Keywords: Carbon emissions, rooftop photovoltaics, solar energy, thermal comfort, aero voltaic panel

1. INTRODUCTION

The demand for alternative energy from renewable sources has continued to rise globally in recent decades, promoted by an increase in environmental awareness and the growing importance placed on sustainability Hence, Renewable energy systems have been the main drivers and will continue to be essential for this transformation towards the achievement of sustainable development goals through the promotion of the security of supply while lowering energy costs, reduction emissions while driving growth, and generation jobs through industrial development. Then, Solar energy is now considered a potential viable choice to replace current fossil fuels in power production in the subtropical region's region, which offers high solar radiation throughout the year. The consistent amount of sunlight averaging 400–600 MJ/m2 per month allows building owners to use the available solar radiation to generate electricity through photovoltaic (PV) systems for daily use [5]. At the same time, this alternative energy is seen as one of the solutions to the problem of utility expenses in residential or administrative buildings because it offers low electricity tariffs in addition to clean energy. Furthermore, the use of clean energy is consistent with the global commitment to reduce carbon emissions and achieve carbon neutrality. The total worldwide power generation capacity of installed PV panels increased by 12% in 2019 and reached a record of 630 GW in total, while the thermal energy generation capacity of installed Solar Thermal (ST)collectors amounted to 480 GW (thermal) in 2019, with China accounting for almost 70% of the total solar thermal capacity [6,7], which corresponds to savings of about 140 million tons of CO_2 per year [6]. In general, PV systems are designed to generate electricity from solar energy that can be an alternative source to the existing power supply from the grid system. However, PV panels also produce unnecessary heat energy during the power generation process, which raises the temperature of PV cells and reduces the installed system's efficiency. PV panels exposed to continuous heating for long periods can also result in structural damage [8]. Currently, various technologies are being proposed to boost the effectiveness of solar PV panels by extracting unwanted heat, using appropriate cooling methods, and good thermal control techniques. The combination of both applications on PV modules results in a photovoltaic thermal system (PVT), which generates electricity and heat simultaneously [9]. A proper cooling method is required to maintain the surface temperature of the PV panel which in turn will increase the overall efficiency of the PV system. In principle, PV cooling technology can be categorized into three, namely passive cooling, active cooling, and a combination of both [10]. Passive cooling techniques involve air,

water, and conductive cooling to remove heat naturally without using energy [11]. Then, Naghavi et al. [12] investigated the natural air movement beneath a PV panel through numerical assessments. Their results showed that temperature differences of 12 ± 5 ◦C and 18 ± 5 ◦C could be obtained when the air gap between the rooftop and panel rear surface was 200 mm and 250 mm, respectively, as compared to the same panel with no gap. A larger air gap allows a greater volume of air to flow and, thus, it can remove heat from the rear side of the panel through convection effectively. Hernandez et al. [13] studied PV panel cooling by placing a panel on the steel roof of an industrial building. The PV panel was cooled by placing air channels underneath it with natural or forced convection cooling. The experimental results showed that the PV panel temperature with the natural convection cooling is around 5 ◦C lower than that without natural cooling on the back. In this case, research can be extended to analyze the temperature on the roof and relate it to the panel temperature since higher roof temperatures can decrease the effectiveness of the cooling effect produced by the natural convection of air because air gets heated by both panels as well as the roof. Although the PV panel with forced convection cooling was able to generate 3–5 % more electricity than the PV panel with natural convection cooling, the forced convection cooling required a fan to maintain the airflow at 4 m/s in the channels. Therefore, comparing the net power produced by both active and passive cooling approaches will be a more pragmatic approach, but in the reviewed study, proper inference could be made, due to the paucity of power consumption data of the fan. Then, Solar energy is an abundant primary energy resource, which can be exploited in cost-competitive and reliable ways for electrical power generation, either with PV technology or thermodynamic cycles in concentrated solar power systems, as well as for heating or cooling purposes through Solar technology systems. Some of the advantages of this renewable resource compared to others, e.g., wind, are its larger predictability on an annual basis and daily [14], the low degradation rate of the components of a solar installation during its lifetime which is generally 20–25 years [15,16], and that this technology rarely underperforms or fails. Shahsavar et al. [17] attached an air channel with a Metal Sheet (TMS) below a glazed PV panel. The air channel was used to cool the ◦C when the solar irradiance was 880 W/m2. The air channel was able to effectively remove the waste heat in the PV panel and generate additional thermal energy. The electrical and thermal efficiencies were around 8 % and 32 %, respectively. However, the authors did not mention the PV temperature change compared to a standalone PV panel, and this hinders solid inferences regarding the effectiveness of the implemented cooling system.

In this regard, there has been a great trend toward the utilization of sustainable energy systems in various applications around the world [18]. Numerous operations, including electricity production, building space heating, hot water generation, drying of crops, desalination and heating, ventilation, air conditioning, and refrigeration (HVAC-R) systems, can be powered by solar energy [20]. Solar energy is concurrently converted into thermal and electrical energy utilizing hybrid photovoltaic/thermal (PV/T) technology [21]. Net-zero constructions can be supported by building-integrated photovoltaic-thermal (BIPV/T) systems, which could generate electrical and thermal energies as well as act as thermal insulators [22]. The need for energy in buildings accounts for the majority of the global energy demand [23]. Building energy usage can account for up to 40% of the global energy supply, with space heating and hot water generation making up the majority of this demand [24]. In 2021, space and water heating accounted for almost half of building energy demand, resulting in 2450 Mt of direct CO2 emissions, according to a publication by the International Energy Agency (IEA) [25]. To lower both the negative impacts of environmental factors and the increasing energy demand, the integration of renewable energy resources into buildings has been frequently used recently [26]. BIPV/T systems can be utilized to help meet these energy demands in buildings. Buildings require both electrical and thermal energy for tasks including space cooling and heating, water heating, ventilation, lighting, and powering various devices. In addition, compared to residential and commercial buildings, industrial structures and activities use more thermal and electrical energy [27]. In essence, it takes a lot of energy to maintain safe, healthy, and comfortable indoor environments in buildings [26]. According to the International Energy Outlook Report [28-30], global energy consumption would enhance by 56% between 2010 and 2040. Buildings accounted for 32% of the world's energy use and 33% of greenhouse Gaz (GHG) emissions in 2012 [30]. This is the outcome of indirect emissions associated with the utilization of energy as well as direct emissions from the in-situ combustion of fossil fuels. This calls for the development of numerous techniques to lower building energy use and, consequently, GHG emissions. Moreover, direct or indirect global GHG emissions in buildings have enhanced by 1% per year since 2010 [31]. While the decarbonization of energy consumption in buildings continues rapidly, all necessary measures must be implemented to attain net zero emissions by 2050 [32]. To meet this goal, 20% of newly developed buildings and existing buildings in the world should be in a carbon-zero state by 2030 according to the International Energy Agency

[31]. By meeting both electrical and thermal energy demands in buildings, hybrid renewable technologies (e.g. photovoltaic-thermal systems, solar-assisted heat pumps) enable buildings to meet the zero-carbon goals. Furthermore, Building PV generation systems can be applied on roofs, Kumar et al. [33] and/or facades, Quesada et al. [34], and the installed PV generation system can share the grid load. There are various types of building loads for different functions, such as cooling, heating, annual electricity demand, air demand, and illumination. Most of these loads are combined with ventilation and air conditioning systems through traditional electric means. In this context, it is possible to achieve low energy consumption in buildings upon integration of PV generation systems.

In hot tropical climate regions, building roofs are exposed to weather and thermal shocks due to solar radiation incidents on the roof envelope. These thermal shocks are often the source of building aging and especially slab roof cracking. The protection of these slab roofs is done by coating them with bitumen. In recent decades, to protect the roof slabs and to make the building more energy efficient, technicians are opting more for photovoltaic coating for the reasons of esthetic evaluation, carbon reduction, and power generation, these main factors are considered in the evaluation of different types of PV roofing. This environmentally friendly new method produces clean energy and makes the bioclimatic building energy-independent.

Based on the existing literature, it can be found that the current utilization of solar energy in buildings is mainly photothermal. However, the use of solar cell plates for coating the slab in buildings is not yet common in hot subtropical climate regions. Thus, this paper focused on the thermal and electrical performances of a photovoltaic roof with an air gap for cooling and protecting simultaneously the slab.

This study aims to innovate and contribute toward a more sustainable hot subtropical climate society through developing alternative coating technologies for cooling rooms and producing non-polluted energy without greenhouse gas emissions.

2.Physical Model and Governing Equations

The physical model considered in Figure 1 is a one-story building, with two air inlets opening (E1 and E2) and two air outlets opening (E6 and Eout). A chimney is integrated into the building for thermosyphon air extraction on the one hand and a horizontal photovoltaic cells plate for the slab roof covering on the other. The model is assumed to be two-dimensional. The photovoltaic cells' plate, placed on the slab, allows on the one hand, to protect the slab against bad weather and thermal shocks, and on the other hand, to provide the building with the necessary electrical energy for the lighting of the rooms and the power supply of the household appliances. Thus, at the exit of the room, the air permanently evacuates the excess heat to cool simultaneously the slab and the photovoltaic cells, for the achievement of thermal comfort in the rooms and the best possible electrical output of the photovoltaic cells. The photovoltaic panel, the glazing, and the absorber of the chimney are the active walls. While the remaining walls are assumed to be adiabatic. The ambient air at the temperature and the velocity U_0 enters the room.

Flow regimes inside the storied building are considered fully laminar, incompressible, and two-dimensional with negligible viscous dissipation and gravity parallel to the ascendant y-axis. The thermophysical properties are considered constant except the density which is approached in the gravity term with the Boussinesq approximation. Radiation and infiltration are neglected in this study. Taking into account the above-mentioned assumptions, the non-dimensional governing equations, written in vorticity – streamlines (ω-ψ) formulation, in Cartesian coordinates are as follows:

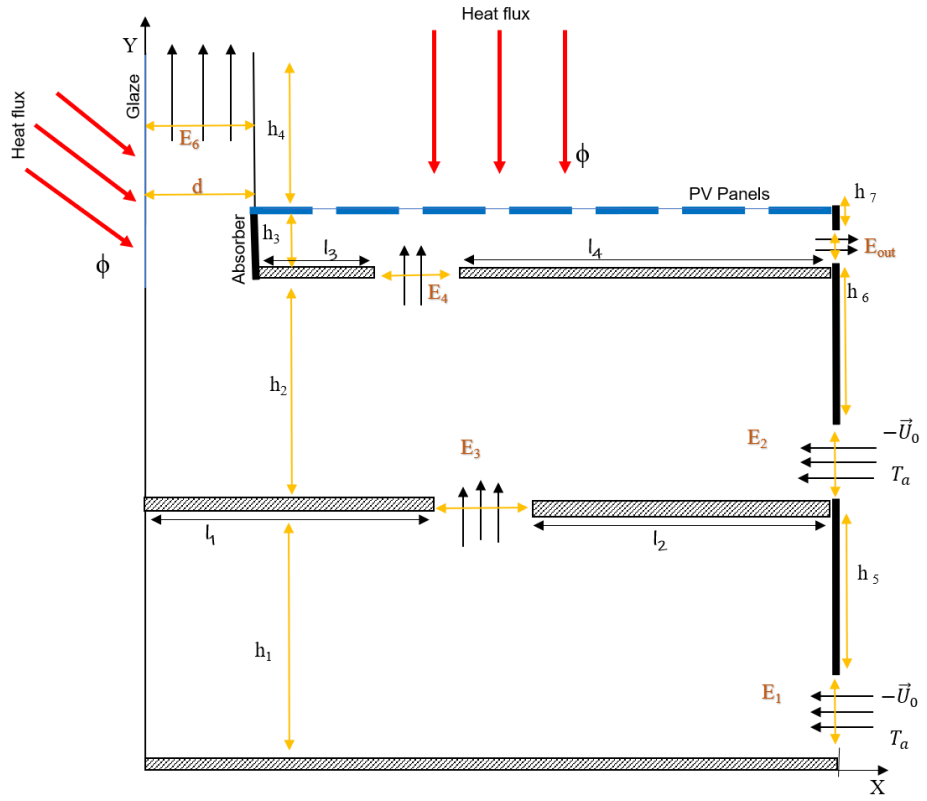

Figure1. Physical model

$$\frac{\partial U}{\partial X}+\frac{\partial V}{\partial Y}=0 \tag{1}$$

$$\frac{\partial \omega}{\partial \tau}+U\frac{\partial \omega}{\partial X}+V\frac{\partial \omega}{\partial Y}=Ri\frac{\partial \theta}{\partial X}+\frac{1}{Re}\left(\frac{\partial^2 \omega}{\partial X^2}+\frac{\partial^2 \omega}{\partial Y^2}\right) \tag{2}$$

$$\frac{\partial \theta}{\partial \tau}+U\frac{\partial \theta}{\partial X}+V\frac{\partial \theta}{\partial Y}=\frac{1}{RePr}\left(\frac{\partial^2 \theta}{\partial X^2}+\frac{\partial^2 \theta}{\partial Y^2}\right) \tag{3}$$

$$\omega=-\left(\frac{\partial^2 \Psi}{\partial X^2}+\frac{\partial^2 \Psi}{\partial Y^2}\right) \tag{4}$$

Boundary Conditions

- Initial conditions: at τ = 0:

$$\theta = \omega = U = V = \psi = 0$$

- at $\tau > 0$

The boundary conditions associated with the problem are found below.

At the first and second air inlet openings E_1 , E_2

$$U=-1; V=0; \theta=0$$

$$Y = 0 \text{ and } 0 < X < \frac{L}{d}, \left.\frac{\partial\theta}{\partial Y}\right|_{Y=0} = 0, U = V = \Psi = 0 ; \omega = -\left.\frac{\partial^2\Psi}{\partial X^2}\right|_{Y=0} \quad (5)$$

$$X = 0 \text{ and } 0 < Y < \frac{h_5}{d}, \left.\frac{\partial\theta}{\partial Y}\right|_{X=0} = 0, U = V = \Psi = 0 ; \omega = -\left.\frac{\partial^2\Psi}{\partial Y^2}\right|_{X=0}$$

$$X = 0 \text{ and } \frac{h_5}{d} < Y < \frac{H}{d}, \left.\frac{\partial\theta}{\partial Y}\right|_{X=0} = -1, U = V = \Psi = 0 ; \omega = -\left.\frac{\partial^2\Psi}{\partial Y^2}\right|_{X=0}$$

$$Y = \frac{h_2}{d} \text{ and } 0 < X < \frac{L_2}{d} \text{ or } \frac{L_3}{d} < X < \frac{L}{d}, \left.\frac{\partial\theta}{\partial Y}\right|_{Y=\frac{h_2}{d}} = 0, U = V = \Psi = 0 ; \omega = -\left.\frac{\partial^2\Psi}{\partial X^2}\right|_{Y=\frac{h_2}{d}}$$

$$Y = \frac{h_5}{d} \text{ and } 0 < X < \frac{L_1}{d} \text{ or } \frac{L_1+E_3}{d} < X < \frac{L}{d}, \left.\frac{\partial\theta}{\partial Y}\right|_{Y=\frac{h_5}{d}} = 0, U = V = \Psi = 0 ; \omega = -\left.\frac{\partial^2\Psi}{\partial X^2}\right|_{Y=\frac{h_5}{d}}$$

At the third air inlet opening E_3 :

$$Y = \frac{h_2}{d} \text{ and } \frac{L_2}{d} < X < \frac{L_3}{d}, \left.\frac{\partial U}{\partial Y}\right|_{Y=\frac{h_2}{d}} = \left.\frac{\partial V}{\partial Y}\right|_{Y=\frac{h_2}{d}} = \left.\frac{\partial\omega}{\partial Y}\right|_{Y=\frac{h_2}{d}} = \left.\frac{\partial\theta}{\partial Y}\right|_{Y=\frac{h_2}{d}} = 0 \quad (6)$$

- At the fourth air inlet opening E_4 :

$$Y = \frac{h_5}{d} \text{ and } \frac{L_3}{d} < X < \frac{L_4}{d}, \left.\frac{\partial U}{\partial Y}\right|_{Y=\frac{h_5}{d}} = \left.\frac{\partial V}{\partial Y}\right|_{Y=\frac{h_5}{d}} = \left.\frac{\partial\omega}{\partial Y}\right|_{Y=\frac{h_5}{d}} = \left.\frac{\partial\theta}{\partial Y}\right|_{Y=\frac{h_5}{d}} = 0 \quad (7)$$

- At the outlet opening E_{out} :

$$X = \frac{L}{d} \text{ and } \frac{h_6}{d} < Y < \frac{h_7}{d}, \left.\frac{\partial U}{\partial Y}\right|_{X=\frac{L}{d}} = \left.\frac{\partial V}{\partial Y}\right|_{X=\frac{L}{d}} = \left.\frac{\partial\omega}{\partial Y}\right|_{X=\frac{L}{d}} = \left.\frac{\partial\theta}{\partial Y}\right|_{X=\frac{L}{d}} = 0$$

- At the chimney outlet opening E6 :
- $Y = \frac{H}{d}$ and $0 < X < \frac{L_1}{d}, \left.\frac{\partial^2 U}{\partial Y^2}\right|_{Y=\frac{H}{d}} = \left.\frac{\partial^2 V}{\partial Y^2}\right|_{Y=\frac{H}{d}} = \left.\frac{\partial^2\omega}{\partial Y^2}\right|_{Y=\frac{H}{d}} = \left.\frac{\partial^2\theta}{\partial Y^2}\right|_{Y=\frac{H}{d}} = 0$
- On the horizontal PV plate :
- $Y = \frac{h_7}{d}$ and $\frac{L_1}{d} < X < \frac{L}{d}$

$$\left.\frac{\partial\theta}{\partial Y}\right|_{Y=\frac{h_7}{d}} = (\alpha\tau)_{PV} - \eta_{él}, U = V = \Psi = 0 ; \omega = -\left.\frac{\partial^2\Psi}{\partial X^2}\right|_{Y=\frac{h_7}{d}} \quad (8)$$

- $X = \frac{L_1}{d}$ and $\frac{h_7}{d} < Y < \frac{H}{d}$

Absorber plate :

- $\left.\frac{\partial\theta}{\partial X}\right|_{X=\frac{L_1}{d}} = -\alpha_{ab}\tau_v, U = V = \Psi = 0 ; \omega = -\left.\frac{\partial^2\Psi}{\partial Y^2}\right|_{X=\frac{L_1}{d}}$ (9)
- Glazing :
- $\left.\frac{\partial\theta}{\partial X}\right|_{X=\frac{L_1}{d}} = -\tau_v\alpha_p, U = V = \Psi = 0 ; \omega = -\left.\frac{\partial^2\Psi}{\partial Y^2}\right|_{X=\frac{L_1}{d}}$ (10)

The heat transfer through the upper horizontal heated solar cells plate is better represented by the Nusselt number, which is a measure of the ratio of the heat transfer by conduction to the flux convected by the cooling fluid. The local Nusselt number on the upper horizontal heated solar cells plate is given by the relation:

$$N_u(p) = \frac{\phi d}{\lambda(T_{PV} - T_a)} \tag{11}$$

The electrical output of solar cells is given by the following relation.

$$\eta_{el} = \eta_{ref}\left[1 - \beta_{ref}\left(\overline{T_{PV}} - T_{ref}\right)\right] + \gamma log_{10} Q_0 \tag{12}$$

For the crystalline silicon PV cells, the coefficient γ is taken to zero [35]. Then the PV cells' electrical efficiency is given as

$$\eta_{el} = \eta_{ref}\left[1 - \beta_{ref}\left(\overline{T_{PV}} - T_{ref}\right)\right] \tag{13}$$

Where $\overline{T_{PV}}$ is a mean temperature along the PV cells plate, T_{ref} is ambiant temperature

2.1. Numerical Procedure

Method Of Solution

In the present work, the nonlinear partial differential governing equations, (1-3), were discretized using a finite difference technique. The first and second derivatives of the diffusive terms were approached by central differences while a second-order upwind scheme was used for the convective terms to avoid possible instabilities frequently encountered in mixed convection problems. The integration of the algebraic equations (2) and (3) was assured by Thomas' algorithm. At each time step, the Poisson equation, Eq. (4), was treated using the Point Successive Under-Relaxation method (PSUR) with an optimum under-relaxation coefficient equal to 0.8 for the grid (121×121) adopted in the present study. Convergence of iteration for stream function solution is obtained at each time step. The following criterion is employed to check for a steady-state solution. Convergence of solutions is assumed when the relative error for each variable between consecutive iterations is below the convergence criterion ε such that $\sum\left|\left(\phi_{i,j}^{k+1} - \phi_{i,j}^{k}\right)/\phi_{i,j}^{k+1}\right| < 10^{-5}$ where ϕ stands for ψ, Θ, ω, k refers to time and i and j refer to space coordinates. The time step used in the computations is $\Delta\tau = 10^{-5}$. To reduce the influence of the mesh on simulation accuracy, mesh independency solutions are assured by comparing different grid meshes for the highest Grashof and Reynolds numbers used in this work (Gr =10^5 and Re = 100). It was found that the differences between meshes of 121 x 121 and 141x141 were not significant for all variables. The results obtained with these grids were comparable to those obtained with other uniform grid sizes of 81x81, 101x101, and 161x161. Thus, a uniform mesh of 121 x 121 was selected. The vorticity computational formula of Woods [36] for approximating the wall vorticity was used: $\omega_P = \frac{1}{2}\omega_{P+1} - \frac{3}{\Delta\eta^2}(\psi_{P+1} - \psi_P)$, where ψ_P and ψ_{P+1} are stream function values at the points adjacent to the boundary wall; η, the normal abscise on the boundary wall.

3. Results and discussion

3.1. Validation

To test the computer code developed for this study, the problem of a ventilated rectangular enclosure with its left and upper walls submitted to a constant heat flux, while the remaining walls are considered adiabatic was studied. Very good agreement is obtained between the test problem solution and the ventilated rectangular enclosure solutions as compared to the work of Raji et al. [37].

Re= 100, Ra = 10^6

A. Raji **Present work**

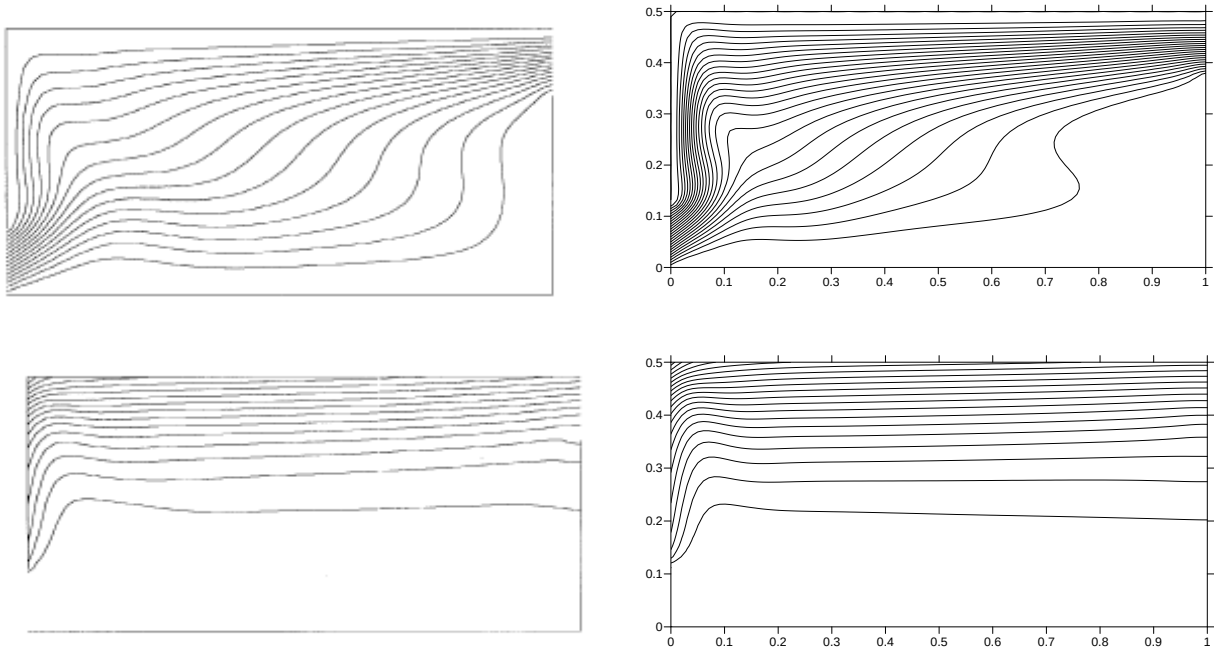

Figure2. Comparison of the present streamlines and isotherms profiles with results from Raji et al. [37]

We chose this physical model of Raji et al.[37] to validate our computer code, because the physical model has the same active wall. The horizontal cold jet enters the enclosure from the bottom of its heated wall and leaves from the top of the other vertical wall with no-slip boundary conditions applied to all the walls. The Reynolds number, Re was set at 100, and for Rayleigh number Ra was set at 106. The numerical analysis predicted values of streamlines and isotherms together with ventilated rectangular enclosure results shown in Figure 2.

Table 1. Numerical model input parameters

Parameters	value
Absorptivity of the glaze, **α**gl	0.05 (-)
The transmittance of the glaze, **τ**gl	0.95 (-)
Absorptivity of PV cells surface, **α**PV	0.89 (-)
Absorptivity of the absorber plate, **α**ab	0.9 (-)
Electrical efficiency at the reference temperature, η_{ref}	0.015(-)
Temperature coefficient of PV cell, β_{ref}	0.0045 K^{-1}
Transmittance of PV cells surface, **τ**PV	0.09 (-)
Reference temperature, T_{ref}	25 ◦C
Width of the vertical chimney, d	0.05(m)
H height of the building	1(m)

3.2. Flow and thermal visualization

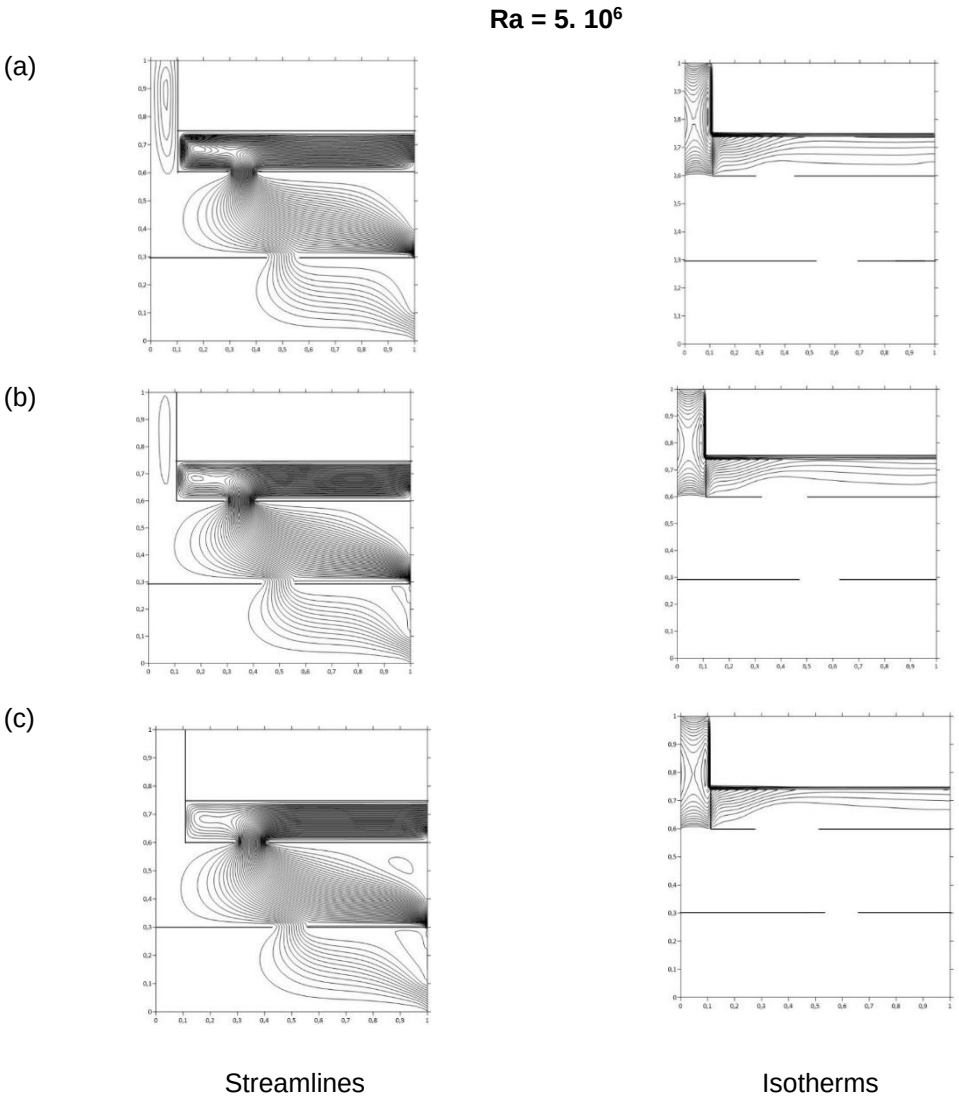

Figure3. Streamlines and isotherms obtained for Ra = 5. 106 and different values of Re: (a) Re =25 (b) Re = 50; (c) Re = 100

Figure 3(a,b,c) illustrates the topology of the flow and the distribution of the thermal field in the ground floor, the floor, and the vertical and horizontal chimneys integrated into the building for useful purposes such as the protection of the slab for its rotting and possible cracks due to thermal shocks and bad weather. Thus, streamlines and isotherms are presented for different values of the Reynolds number with a fixed Rayleigh number. The presence of open lines can be seen in the rooms while open lines and closed cells are in the chimneys. The coexistence of open and closed lines demonstrates sufficiently the manifestation of mixed convection phenomenon in horizontal and vertical chimneys integrated into the building. It can be noted for the weak values of the Reynolds number, the natural convection closed cells are present in the vertical chimney. This situation shows that air molecules that have not been charged enough energy recirculate. In addition, the molecules of the coolant fluid pass through the duct of the horizontal chimney protecting the roof of the slab.

The air molecules that extract excess heat from the rooms and roof of the slab mostly pass under the photovoltaic solar panel. This permanent movement of air in the channel created between the slab roof and the active wall of the horizontal protective chimney enables the ventilation of the slab and the photovoltaic cells to achieve two main objectives. Improving the electrical efficiency of photovoltaic cells, and thermal comfort in the living spaces in the rooms of the multi-story building. The isotherms are concentrated in the chimneys. This aspect shows that these are the areas where heat transfer takes place intensively. It may be noted that the isotherms are parallel in the horizontal protective chimney. This situation can be explained that conduction is the main mode of heat transfer highlighted on the photovoltaic panel. In addition, mixed convection has always been manifested by the bifurcation of the isotherms in the channel of the vertical chimney integrated into the building. It can be concluded that mixed convection further improves the ventilation of the rooms of the storied building and the aero voltaic panel.

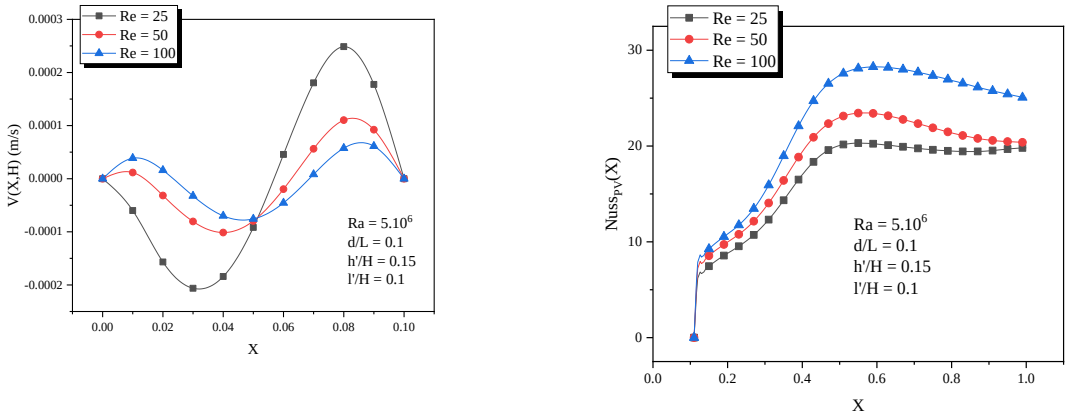

a) The vertical component of velocity

b) Nusselt number along the aero voltaic panel

Figure 4. Variation of velocity and local Nusselt number for different Reynolds number

Figure 4(a) shows the variation of the vertical component of velocity versus Reynolds number. In the first half of the duct of the integrated vertical chimney into the building, the outlet velocity of the coolant fluid is an increasing function of the Reynolds number, while it is a decreasing function in the second half of the channel. This situation means that the air molecules near the active glaze wall do have not the necessary energy to leave the chimney, and then the advection phenomenon is manifested, the reason for which, velocity values are negative. The positive values of the vertical velocity in the second half of the vertical chimney show that it is an area where the thermosiphon phenomenon of the air for the multi-story building cooling is manifested.

In Figure 4(b), the local Nusselt number along the active PV cells plate is an increasing function of the Reynolds number. One can note that the higher is Reynolds number, the higher the Nusselt number. It means that the horizontal protective PV cell plate is very vented via the inlet fresh air. Hence the heat excess along the PV cells plate is dissipated. The aero-voltaic panel temperature is always close to the ambient air temperature.

3.3. Influence of Rayleigh's number

The effect of the Rayleigh number ($10^4 \leq Gr \leq 10^7$) for a fixed Reynolds number (Re = 50) is presented in Figure 5 (a,b,c) illustrates the variation in streamlines and isotherms for different values of the Rayleigh number. The flow structure varies very little as the Rayleigh number increases. However, mixed convection is manifested in the system by the coexistence of the open and the enclosed lines. The increase in the size of the counterrotating cells in the vertical chimney indicates an increase in natural convection, and the increasing number of enclosed streamlines under the upper horizontal photovoltaic cell plate indicates the domination of forced convection in this area. The Rayleigh number influences the system by significantly increasing its temperature in the vicinity of heat sources. Fig 5 (a,b,c) shows clearly the increase in temperature stratification. Increasing the Rayleigh number reduces heat transfer to the photovoltaic cells and lowers their electrical efficiency. On the other hand, increasing the Rayleigh

number favors heat transfer in the vertical chimney and increases the vertical component of the velocity at the vertical chimney exit. Figure 6 (a) clearly shows that the vertical component of velocity at the exit of the vertical chimney is an increasing function of the Rayleigh number. In the first half of the duct of the vertical chimney, one can observe the advection phenomenon for the negative value of velocity, whereas the thermosiphon phenomenon is observed for the positive value of the velocity in the second half of the duct of the vertical chimney near the active photovoltaic panel.

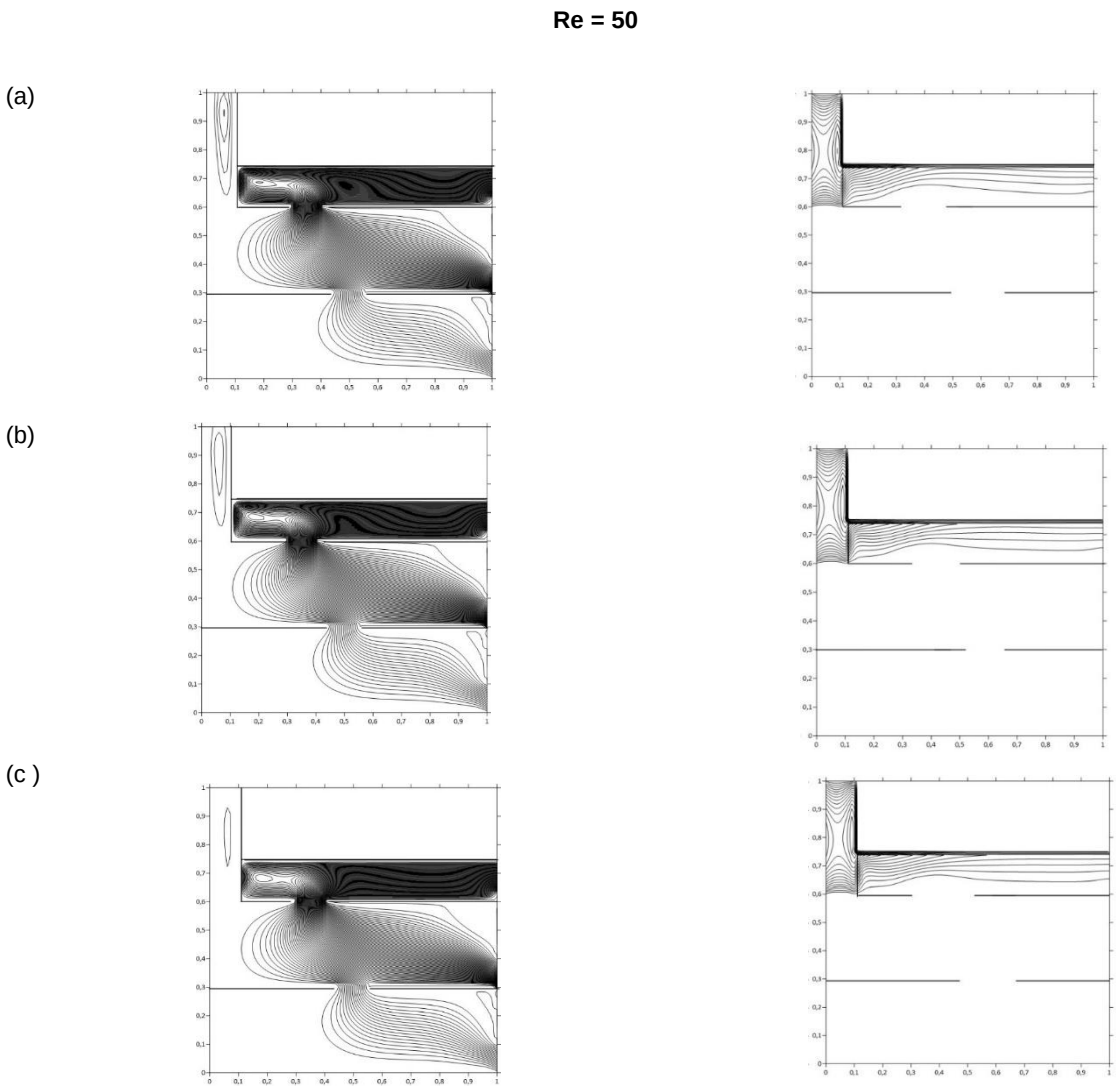

Figure 5. Variation of streamlines and isotherms obtained for Reynolds number Re = 50; and various Rayleigh number a) Ra = 4.10^6 b) Ra = 8.10^6 c) Ra = 10^7

The Rayleigh number influence on the present work shows that increasing the Rayleigh number most adversely affects the electrical performance of the solar cells in the horizontal photo voltaic chimney. The local Nusselt number along the heated photovoltaic plate is a decreasing function of the Rayleigh number as shown in Figure 6 (b). This variation of the local Nusselt number proves that the local Nussselt number is inversely proportional to the heated flux which is correlated with the Rayleigh number. By increasing the Rayleigh number, the dimensionless temperature increases, consequently the local Nusselt number decreases.

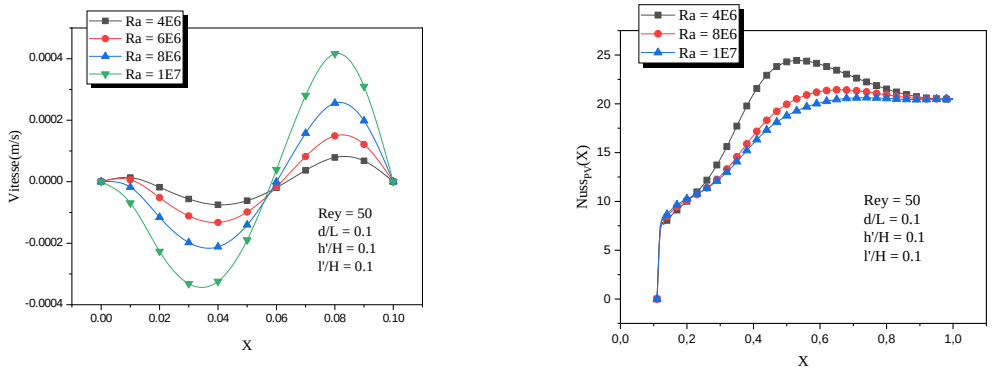

a) Vertical velocity component

b) Local Nusselt number along PV cells plate

Figure 6. Variation of velocity and local Nusselt number versus Rayleigh number

For the natural convection in the vertical as the horizontally integrated chimneys into the storied building, the flow and temperature distributions are influenced by many geometrical factors, such as the channel size, the heated plate height, and the inlet or outlet opening size. In this section, the effect of these factors will be assessed to determine the range of these main geometrical factors for providing simultaneously electricity and thermal comfort in the storied building.

3.4. Influence of PV plate height on the Roof

The height between the roof and the PV plate plays a key role in the ventilation of the upper horizontal solar chimney. Then, Figure 7(a,b,c) gives more illustration of the movement of the coolant fluid in the bioclimatic building. Hence, in Figure 7(a), where the duct of the horizontal chimney is weak, one can observe the simultaneous existence of the closed cells and the open lines in the bioclimatic storied building. This size of the horizontal hybrid photovoltaic-thermal chimney promotes heat exchange between the roof and the PV cell plate. The thermal plume is observed in the gaps in the chimneys. Due to a large cold zone obtained for maintaining the thermal comfort in the rooms of the storied building. The isotherms' bifurcations indicate the mixed convection phenomenon in the vented storied building, due to the existence of open lines and the closed cells in the room and the chimneys. Then, one can observe in Figure 7(b), and Figure 7(c), that when increasing the gap of the horizontal solar chimney, the size of the closed cells decreases. This situation prevents the existence of Rayleigh Bernard's natural convection closed cells in the rooms. Hence the forced flow is more dominant than the natural convection, due to a large number of open lines in both last horizontal chimney designs.

Re = 50, Ra = 5.10^6

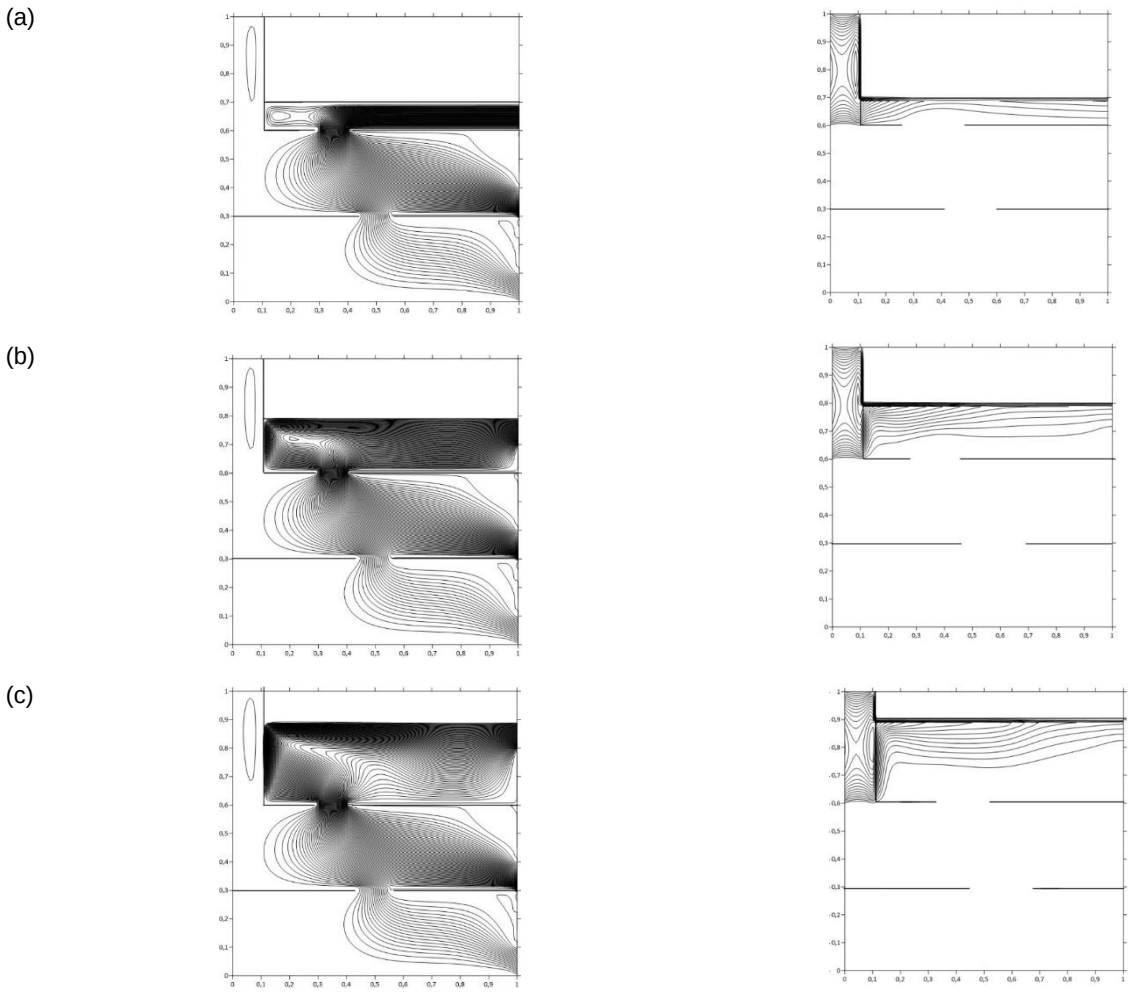

Figure 7. Streamlines and isotherms for different heights of the PV plate on the roof a) h'/H = 0,7; b) h'/H = 0,8; c) h'/H = 0,9

In Figure 8(a), the outlet velocity decreases to attain the minimum value in the first half of the vertical chimney width, before it increases to attain the maximum value in the second half of the vertical chimney width. No sleep conditions are observed along the limited solid walls along the chimneys. One can observe the manifestation of the backflow or reverse flow phenomenon in the first half of the width of the vertical chimney. This tendency can be explained that the outlet velocity in the vertical chimney is a decreasing function of the PV plate height on the roof in the first half of the vertical chimney width, whereas it is an increasing function of the same geometrical parameter in the second part of the width of the vertical chimney.

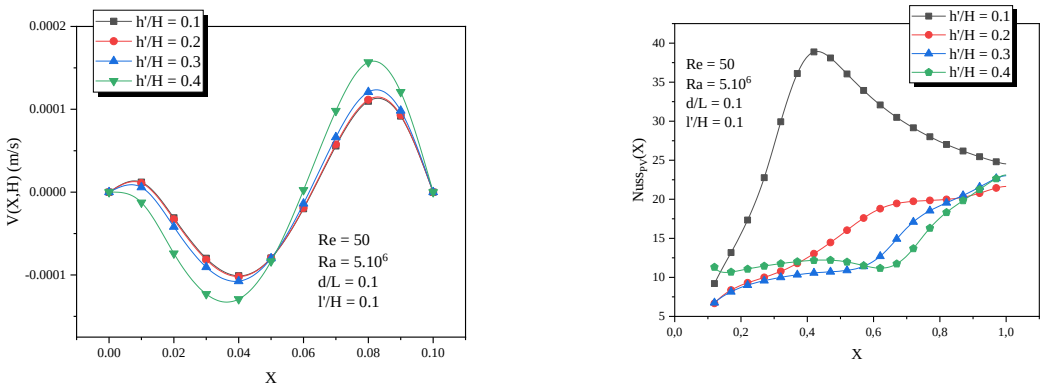

(a) The vertical component of outlet velocity (b) Local Nusselt number along the PV plate

Figure 8. Variation of the outlet velocity and local Nusselt number versus PV plate height on the slab

The height of the PV plate on the roof is an important controlling parameter of the heat exchange in the depth of the horizontal chimney. Hence, Figure 8(b), indicates that the intensity of the heat exchange is a decreasing function of the height of the PV plate on the roof. The local Nusselt number is an inverse relation to the dimensionless temperature. Then, the smaller the height, the higher is Nusselt number along the heated PV cell plates. The variation of Nusselt number along the PV cells plate in the horizontal chimney gives more explication that the heat is more exchanged when the PV cells plate is perfectly vented. Furthermore, the positioning of the air outlet opening under the photovoltaic panels is a key parameter for heat evacuation. Thus, the thermal and dynamic fields were appreciated for two positions of the outlet opening. The outlet opening is positioned between the two elbows (configuration 1) or the outlet opening without the elbows, (configuration 2). A comparative study in terms of the intensity of heat transfer throughout the field of photovoltaic panels was made. This study reveals that configuration 2 offers a better flow of hot air under the photovoltaic panels and confers a good variation in the local Nusselt number along the field of photovoltaic panels, Figure 9 (a).

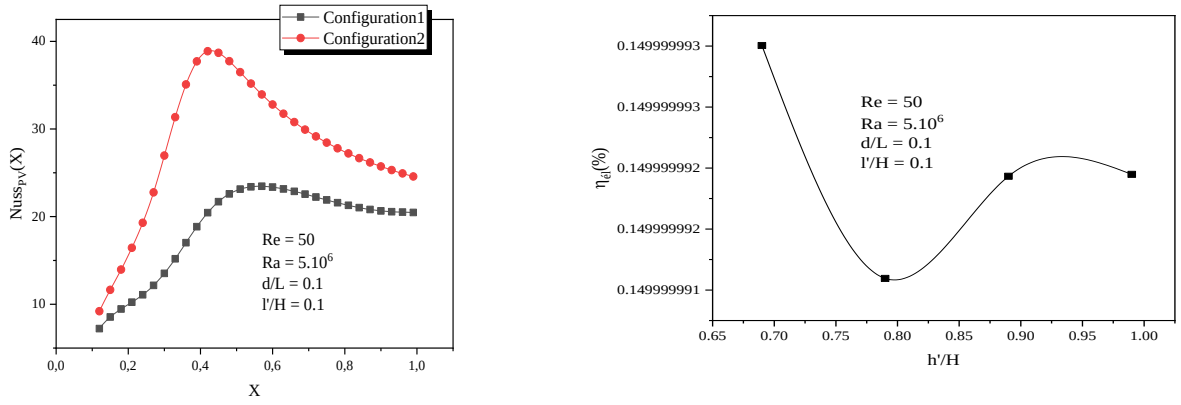

(a) Nusselt number along PV cells plate (b) PV cells' electrical output

Figure 9. Variation of Nusselt number and electrical output versus PV plate height on the roof.

3.4. Effects of aspect ratio and outlet opening size under the PV plate.

The exhaust opening of the polluted and hot air below the photovoltaic plate plays an important role in the slab and solar cells' cooling. Heat transfer intensity is a decreasing function of the outlet opening of hot and polluted air. The lower the opening between the photovoltaic plate and the slab, the greater the Nusselt number. This situation explains why the extract of excess heat at the level of the protective photovoltaic plate of the slab, is increased with the small dimensions of this opening of exit of the hot air of the building, Fig ure10.

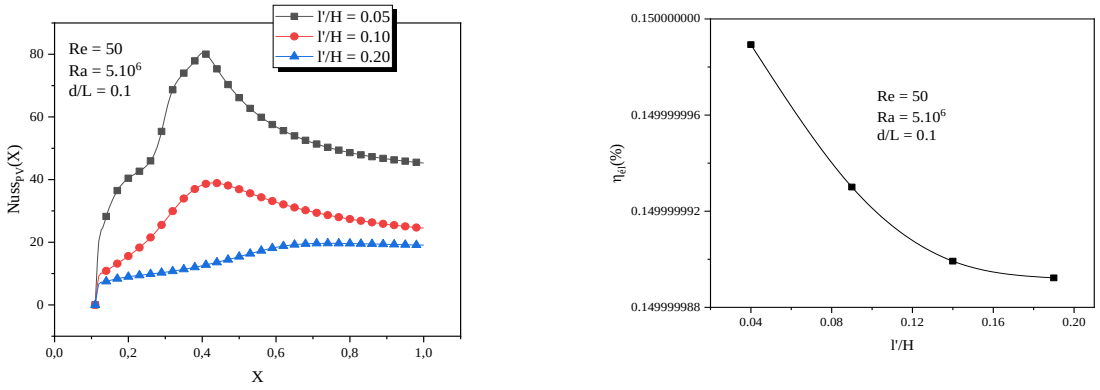

(a) Nuselt number along PV cells plate (b) PV cells' electrical output

Figure10. Variation of Nusselt number and PV cells electrical output versus outlet opening size under the PV plate on the slab

The cooler the solar cells, the greater the electrical energy generated. This aspect is well elucidated by Figure 10 (b), which shows the variation in the electrical efficiency of the cells on the photovoltaic plate protecting the slab against thermal shocks. One can observe that the PV cells' electrical efficiency is an increasing function of the geometrical aspect ratio, Figure 11, whereas it is a decreasing function of the size of the outlet opening under the PV cells plate on the slab., Figure 10 (b)

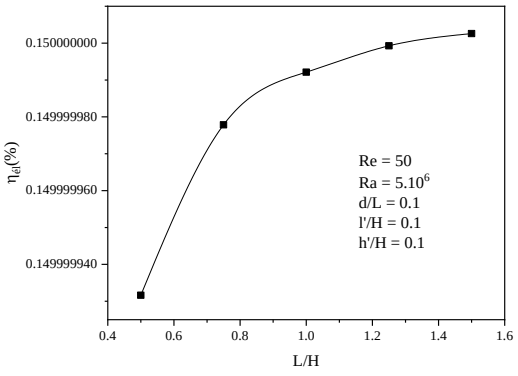

Figure 11. Variation of PV cells' electrical output versus aspect ratio

CONCLUSION

In the present study, authors modeled the airflow in a transient laminar regime, in a room equipped with a vertical chimney, whose slab roof is protected by a horizontal photovoltaic chimney. The results were made to compare the

effects of key parameters for the thermal and electrical performances of the horizontal protective hybrid thermal photovoltaic collector, installed on the slab roof of the building. The comparative study of the performance of the photovoltaic collector showed that the larger air gap between the photovoltaic panel and the slab roof enables a greater volume of air to flow. Thus, the coolant fluid removes heat from the rear side of the protective photovoltaic panel through mixed convection to provide the best electrical efficiency. One can conclude that the photovoltaic panel coatings' technology makes it possible to protect the roof of the slab of the building, produce electricity for domestic or industrial needs, and subsequently make the passive air conditioning of the rooms.

Acknowledgments

This work was supported by the Centre d'Excellence Régional sur la Maîtrise de l'Electricité (CERME) of the University of Lome. Through these words, the authors express their acknowledgment of CERME.

Nomenclature

CP	Specific heat (J. kg^{-1}. K^{-1})
L	Building Length (m)
H	Building height (m)
h'	The relative height of the PV cells plate (m)
L1	Length of the room before opening E3 (m)
L3	Length of the story before opening E4 (m)
e	Inlet /outlet opening (m)
A	The geometrical aspect ratio of the building (A = L/H)
E	Inlet/outlet opening aspect ratio ($E = e/d$)
g	Gravitational acceleration (m.s-2)
n	Coordinate in a normal direction
$N_u(p)$	Nusselt number$N_u(p) = \frac{\phi d}{\lambda(T_{PV}-T_a)}$
t	Time (s)
T	Temperature(K)
Ta	Ambient air temperature (K)
u, v	Velocity component in x and y directions (m.s-1)
U, V	Dimensionless velocity component in X and Y directions; U= u/u0, V = v/u0
u0	Air inlet velocity (m.s-1)
x,y	Coordinates defined in Fig. 1 (m)
X, Y	Dimensionless spatial coordinates; X = x/d, Y = y/d
Re	Reynolds number: $Re = \frac{\rho v_0(2d)}{\mu}$
Pr	Prandlt number:$Pr = \mu Cp/\lambda$
Nu	Nusselt number: $Nu = \frac{\emptyset d}{\lambda(T-T_a)} = \frac{1}{\theta}$
Gr	Grashof number $Gr = \frac{g\beta\emptyset d^4}{\lambda V^2}$
Ri	Thermal Richardson number ($Ri = Gr / \mathrm{Re}^2$)
Greek symbols	
θ	Dimensionless temperature $\theta = \frac{\lambda(T-T_a)}{\emptyset d}$
τ	Dimensionless time $\tau = \frac{u_{0t}}{d}$
Ψ	Dimensionless stream function: $\Psi = \frac{\psi}{du_0}$
ω	Dimensionless vorticity: $\omega = \frac{\Omega d}{u_0}$
Ω	Vorticity(s-1)

ψ	Stream function (m.s-2)
β	Thermal expansion coefficient (K-1)
β_{ref}	Temperature coefficient of PV cell
η_{el}	Electrical efficiency
ρ	Air density (kg.m-3)
λ	Thermal diffusivity of the air (W.m-1. K-1)
μ	Dynamic viscosity of the air (kg .m-1. s-1)
ϕ	Solar radiation (W.m-2)
ν	Cinematic viscosity (m2.s-1)
subscripts	
f	Fluid (air)
P	Plate
ab	Absorber
PV	Photovoltaic
gl	glaze
GHG	Greenhouse Gaz
TMS	Thin Metal Sheet
ST	Solar Thermal

REFERENCES

[1] The United Nations. Rio Declaration on Environment and Development.1992.http://www.unesco.org/education/pdf/RIO_E.PDF. [Accessed 25 June 2017].

[2] UNEP Climate Action. COP 21 Paris France sustainable innovation forum. 2015. http://www.cop21paris.org. [Accessed 25 June 2017].

[3] EG Science. Background on impacts, emission pathways, mitigation options, and costs. The 2◦C target. Information Reference Document; 2008.

[4] European Commission. Best practices on renewable energy self-consumption. 2015. Brussels.

[5] Mekhilef, S., Safari, A., Mustaffa, W.E.S., Saidur, R., Omar, R., Younis, M.A.A., 2012. Solar energy in Malaysia: Current state and prospects. Renew. Sustain. Energy Rev. 16 (1), 386–396

[6] Weiss W, Spokr-dur M. Solar heat worldwide. 2020.

[7] statista. Cumulative installed solar PV capacity worldwide from 2000 to 2018 (in megawatts). 2019. https://www.statista.com/statistics. [Accessed 23 December 2020].

[8] Suresh, A.K., Khurana, S., Nandan, G., Dwivedi, G., Kumar, S., 2018. Role on nanofluids in cooling solar photovoltaic cells to enhance overall efficiency. Mater. Today: Proc. 5 (9), 20614–20620.

[9] Ghadiri, M., Sardarabadi, M., Pasandideh-fard, M., Moghadam, A.J., 2015. Experimental investigation of a PVT system performance using nano ferrofluids. Energy Convers. Manage. 103, 468–476.

[10] Sato, D., Yamada, N., 2019. Review of photovoltaic module cooling methods and performance evaluation of the radiative cooling method. Renew. Sustain. Energy Rev. 104, 151–166.

[11] aya-Lara, O., McDonald, A., 2018. Enhancing PV modules' efficiency and power outputusing i-concept cooling technique. Energy Rep. 4, 357–369.

[12] Naghavi MS, Esmaeilzadeh A, Singh B, Ang BC, Yoon TM, Ong KS. Experimental and numerical assessments of underlying natural air movement on PV modules temperature. Sol Energy 2021;216:610–22.

[13] Hernandez RM, Cascales JRG, Garcia FV, Kaiser AS, Zamora B. Improving the electrical parametersof a photovoltaic panel by means of an induced or forced air stream. Int J Photoenergy 2013 :1–10.

[14] Graabak I, Korpås M. Variability characteristics of European wind and solar power resources—a review. Energies 2016;9:449. https://doi.org/10.3390/ en9060449.

[15] IEA. Photovoltaic power systems technology collaboration Programme. PVPS annual report. 2016.

[16] Mauthner F, Weiss W, Spork-Dür ¨ M. Solar heat worldwide. Market and Contribution to the energy supply 2014. In: Solar heating and cooling Programme. SHC); 2016.
[17] Shahsavar A, Ameri M, Gholampour M. Energy and exergy analysis of a Photovoltaic-Thermal collector with natural airflow. J Sol Energy Eng 2012;134: 1–10.
[18] A.Q. Al-Shetwi, Sustainable development of renewable energy integrated power sector: Trends, environmental impacts, and recent challenges, Science of The Total Environment 822 (2022), 153645.
[19] R. Dutta, K. Chanda, R. Maity, Future of solar energy potential in a changing climate across the world: A CMIP6 multi-model ensemble analysis, Renewable Energy 188 (2022) 819–829.
[20] F. Selimefendigil, C. S¸irin, Experimental investigation of a parabolic greenhouse dryer improved with copper oxide nano-enhanced latent heat thermal energy storage unit, International Journal of Energy Research 46 (3) (2022) 3647–3662.
[21] M. Salem Ahmed, A.S.A. Mohamed, H.M. Maghrabie, Performance evaluation of combined photovoltaic thermal water cooling system for hot climate regions, Journal of Solar Energy Engineering 141 (4) (2019).
[22] G. Yu, H. Yang, Z. Yan, M.K. Ansah, A review of designs and performance of façade-based building integrated photovoltaic-thermal (BIPVT) systems, Applied thermal engineering 182 (2021), 116081.
[23] U. Eicker, Energy efficient buildings with solar and geothermal resources, John Wiley & Sons, 2014.
[24] K. Sezen, A.D. Tuncer, A.O. Akyuz, A. Gungor, Effects of ambient conditions on solar assisted heat pump systems: A review, Science of the Total Environment 778 (2021), 146362.
[25] International Energy Agency (IEA) (2022). Heating, IEA, Paris https://www.iea. org/reports/heating, License: CC BY 4.0.
[26] A. Ahmed, T. Ge, J. Peng, W.C. Yan, B.T. Tee, S. You, Assessment of the renewable energy generation towards net-zero energy buildings: a review, Energy and Buildings 256 (2022), 111755.
[27] Rashid, F., Hoque, M. E., Peash, K. I., Faisal, F. (2030). Performance analysis and investigation forthe development of energy-efficient buildings. Energy, 9, 10.
[28] C. Fan, F. Xiao, S. Wang, Development of prediction models for next-day building energy consumption and peak power demand using data mining techniques, Applied Energy 127 (2014) 1–10.
[29] K.K.W. Wan, D.H.W. Li, D. Liu, J.C. Lam, Future trends of building heating and cooling loads and energy consumption in different climates, Building and Environment 46 (2011) 223–234.
[30] M.W. Akram, M.F. Mohd Zublie, M. Hasanuzzaman, N.A. Rahim, Global Prospects, Advance Technologies and Policies of Energy-Saving and Sustainable Building Systems: A Review, Sustainability 14 (3) (2022) 1316.
[31] International Energy Agency, Tracking Buildings 2021, Available at: https://www.iea.org/reports/tracking-buildings-2021, 2021.
[32] International Energy Agency, Buildings, IEA, Paris, 2022 https://www.iea.org/ reports/buildings.
[33] Kumar, N.M., Sudhakar, K., Samykano, M., 2018. Performance of thin-film BIPV as a double-sloped pitched roof in buildings of Malaysia. Energy Sources, Part A Recover. Util. Environ. Eff. 40, 2476–2484. doi:10.1080/15567036.2018.1502847.
[34] Quesada, G., Rousse, D., Dutil, Y., Badache, M., Hallé, S., 2012. A comprehensive review of solar facades. Opaque solar facades. Renew. Sustain. Energy Rev. 16, 2820–2832. doi :10.1016/j.rser.2012.01.078.
[35] K. Sabrina, «Etude numérique de la ventilation naturelle par la cheminée solaire,» UNIVERSITE ABOU BEKR BELKAÏD - TLEMCEN, 2013. Mémoire de Master.
[36] Woods L.C., A note of numerical solution of fourth differential equations, Aero. Q. 5 (1954) 176-l84.
[37] Raji, A., Hasnaoui, M., 2000. Mixed convection heat transfer in ventilated cavities with opposing andassisting flows. Eng. Comput. Int. J. Comput.-Aided Eng. Softw. 17, 556–572.

DOI: https://doi.org/10.15379/ijmst.v10i3.2705